

Chapter 1.

Introduction to Electrochemical, Quartz Crystal Microbalance and Structural Techniques Used to Characterise Redox Reactions

1.1. Introduction

The focus of much of this thesis is on the investigation of a variety of solid-state reactions by electrochemical and quartz crystal microbalance measurements. Electrochemistry provides a powerful means of studying solid state reactions, in particular solid state phase transformations. However, there is a strong need for ancillary techniques which can also acquire data in real time and which can provide corroborative or other evidence of the underlying reaction schemes. Consequently, the possibility of adapting the Quartz Crystal Microbalance (which measures mass attached to the electrode) to probe kinetics of electrochemically-driven solid state phase transformations has been explored in a number of complexes of technological interest.

An example of a solid state redox reaction is given below:



What distinguishes this reaction from a solution phase reaction is the ion transfer process (intercalation). Standard electrochemistry will give no direct information on this ion transfer process as only “the electrons” are being measured. However, the quartz crystal microbalance which measures attached surface mass will be able to measure this ion transfer process and provide important additional information. The first part of this introduction chapter will therefore provide an overview of electrochemical techniques used in this thesis. This is followed by the principles of solid state studies, the use of the electrochemical quartz crystal

microbalance and techniques to characterise structures prior to and after electrochemical oxidation and reduction.

The need to characterise the morphology of the attached crystals can be important in studying these systems. In particular morphology changes may occur upon oxidation or reduction or even upon addition of reagents to the solution phase (Chapter 6). This morphology can be characterised using microscopy. Crystal structures of these solid materials are also of interest in elucidating these solid state mechanisms. For this purpose, powder X-ray diffraction and single crystal X-ray diffraction are used through these studies. The introductory chapter therefore also contains brief details of the structural tools used to characterise the nature of the solid state changes that occur during the course of the electrochemical experiments.

1.2. Cyclic Voltammetry.

The determination of the mechanisms underlying an oxidation or reduction process can be achieved through a variety of electrochemical methods. The most common and perhaps most straightforward technique used is cyclic voltammetry [1]. This involves applying an external triangular voltage to the electrochemical cell, sweeping through a potential range and reversing the direction of the sweep in a cyclic fashion (see Figure 1.1). The resulting current (I) is monitored as a function of applied potential (E) to give the I - E curve which in this kind of experiment is called a cyclic voltammogram.

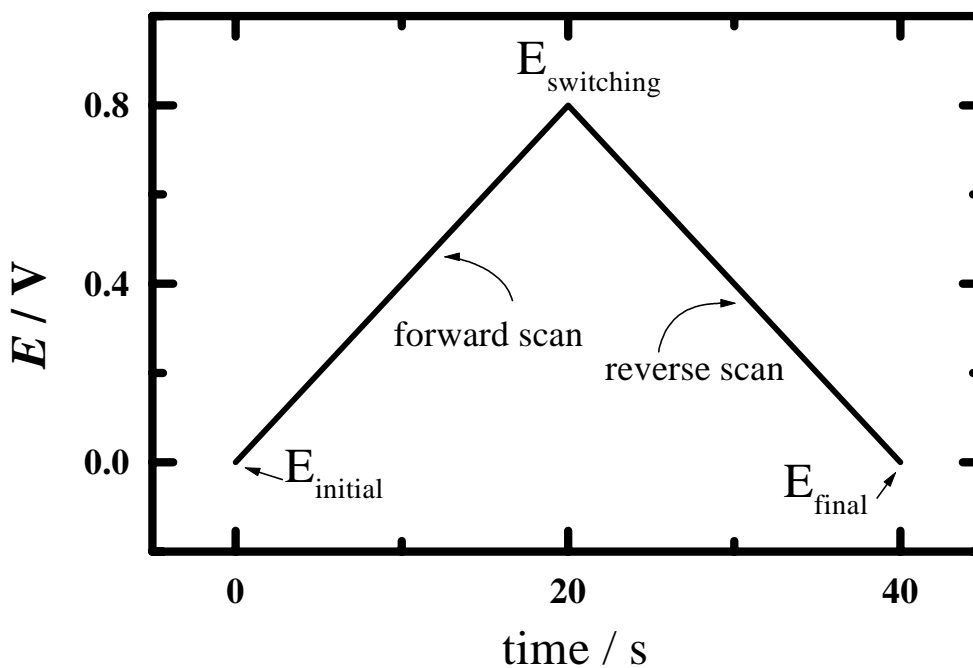


Figure 1.1. Waveform Excitation Signal for Cyclic Voltammetry.

Typically a three electrode potentiostated system is used: a working electrode, reference electrode and a counter electrode. The current flows between the working electrode and the counter electrode (ideally the electronic circuitry ensures that no current will flow through the reference). The potential is controlled relative the reference electrode which is placed as close to the working electrode as possible to reduce ohmic (IR) potential drop.

1.3. Solution Phase Voltammetry. Figure 1.2 shows a solution phase voltammogram simulated using Digisim [2]. This process could be for example the oxidation of ferrocene $[\text{Fe}(\text{C}_5\text{H}_5)_2]$ in an organic solvent. In this case, both the oxidised and reduced forms of the $[\text{Fe}(\text{C}_5\text{H}_5)_2]^{0/+}$ redox couple are soluble in the

solvent. The value of the initial potential is 0.2 V and chosen such that there is no electrochemical process occurring and hence no initial current flow.

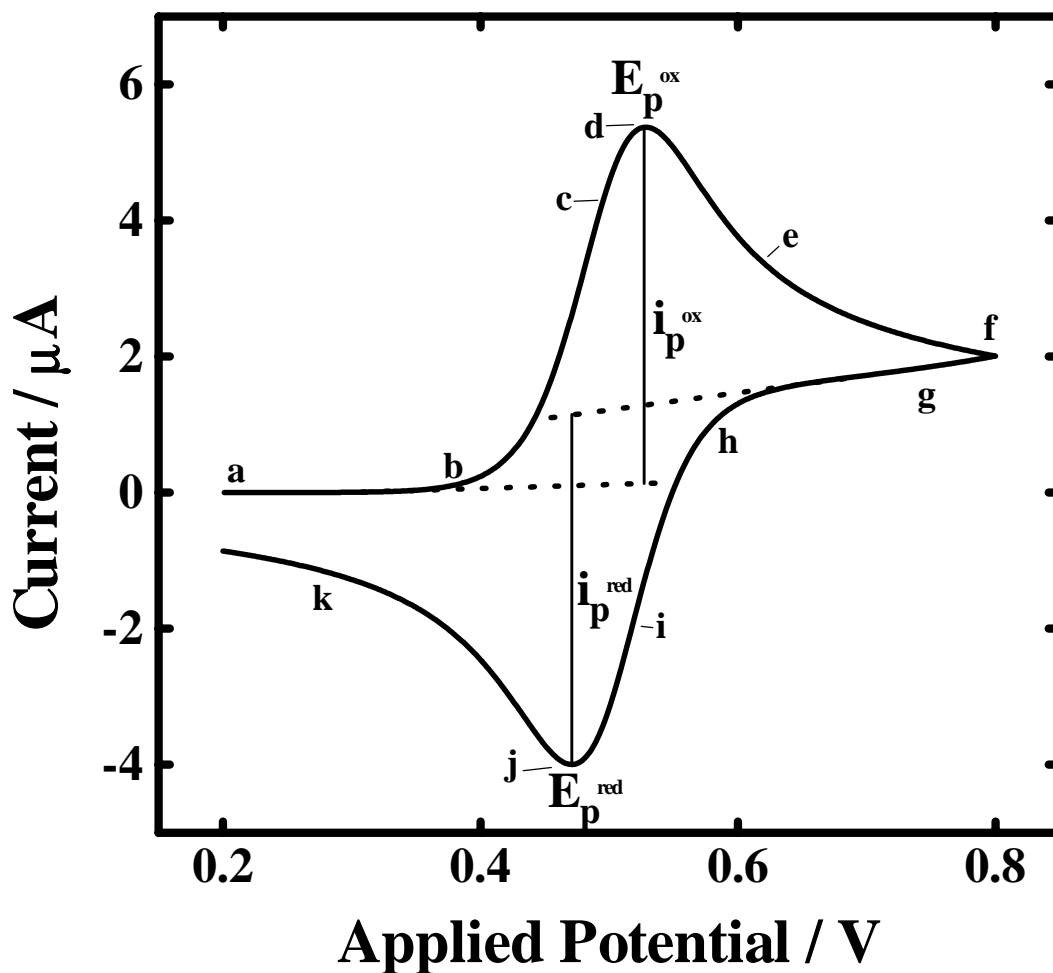
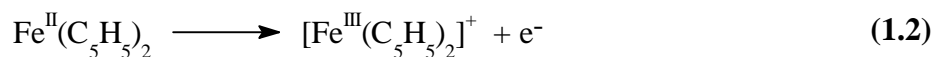
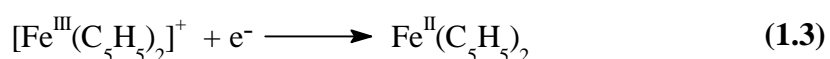


Figure 1.2. Simulated cyclic voltammogram of 0.5mM $[\text{Fe}(\text{C}_5\text{H}_5)_2]$ in organic solvent. Electrode, area = 2.54 mm². Scan rate of 100 mVs⁻¹.

The potential is then initially swept in a positive direction in order to oxidise the starting compound:



Note, in Figure 1.2, the positive direction on the current scale is oxidation current. The oxidation current increases rapidly (b to d) until the concentration of $\text{Fe}^{\text{II}}(\text{C}_5\text{H}_5)_2$ at the electrode surface is significantly diminished. This causes the current to peak at a maximum value E_p^{ox} and then decay (d to g) as controlled by the rate diffusion of $\text{Fe}^{\text{II}}(\text{C}_5\text{H}_5)_2$ from the bulk. The scan direction is switched at about 0.8 V and then the potential is swept in a negative direction in order to reduce the newly formed $[\text{Fe}^{\text{III}}(\text{C}_5\text{H}_5)_2]^+$. Oxidation current is still flowing even though the potential is now being swept in a negative direction. It is not until the potential is negative enough to reduce the $[\text{Fe}^{\text{III}}(\text{C}_5\text{H}_5)_2]^+$ that reduction currents are observed:



Again the current rapidly increases (i to k) to give a maximum value of E_p^{ox} as the concentration of $[\text{Fe}^{\text{III}}(\text{C}_5\text{H}_5)_2]^+$ is depleted at the electrode surface and diffusion control gives rise to current decay after a maximum value (j to k).

For a reversible process (equilibrium established within the timescale of the experiment) the formal reduction potential E^0 is approximately half way between the peaks' potentials [1]:

$$E^{0'} = \frac{E_p^{\text{ox}} + E_p^{\text{red}}}{2} \quad (1.4)$$

The separation between peak potentials (E_p^{ox} and E_p^{red}) is determined by the number of electrons transferred in the electrode reaction (n) [1]:

$$\Delta E_p = E_p^{\text{ox}} - E_p^{\text{red}} \cong \frac{0.056}{n} \quad (\text{at } 25^\circ\text{C}) \quad (1.5)$$

Slow electron transfer (irreversibility) or uncompensated resistance (IR drop) will cause the separation (ΔE_p) to increase.

The values of i_p^{ox} and i_p^{red} should be identical for a reversible couple.

Chemical irreversibility, in which a chemical reaction is coupled to the electrode process causes departures from unity for the ratio $i_p^{\text{ox}} / i_p^{\text{red}}$.

Finally, the peak current for a reversible system is given by the Randles-Sevcik equation [1]:

$$i_p = (2.69 \times 10^5) n^{3/2} A D^{1/2} C v^{1/2} \quad (\text{at } 25^\circ\text{C}) \quad (1.6)$$

where i_p is the peak current (A), n is the electron stoichiometry, A is electrode area (cm^2), D is the diffusion coefficient ($\text{cm}^2 \text{s}^{-1}$), C is the concentration (mol cm^{-3}) and v is the scan rate (V s^{-1}).

1.4. Solid State Voltammetry.

The typical form of solid state voltammetry of interest in this thesis involves crushing a redox active compound into a fine powder and abrasively rubbing this compound onto the electrode. The voltammetry of the surface immobilised (imbedded) compound is carried out when the electrode is placed in a solvent (eg water) in which the compound is not soluble. When the redox reaction occurs within the solid the electrolyte ion provides charge neutralisation. A range of responses can be observed which usually are quite different to that described above for solution phase voltammetry.

1.4.1. Nucleation and Growth Controlled Processes.

One form of solid state response is illustrated in Figure 1.3 [3-4]. This is the solid state voltammetry for the reduction of TCNQ(solid) to TCNQ⁻ (solid) [3-7] on a RAMTM electrode [8] in contact with 1M KCl(aq).

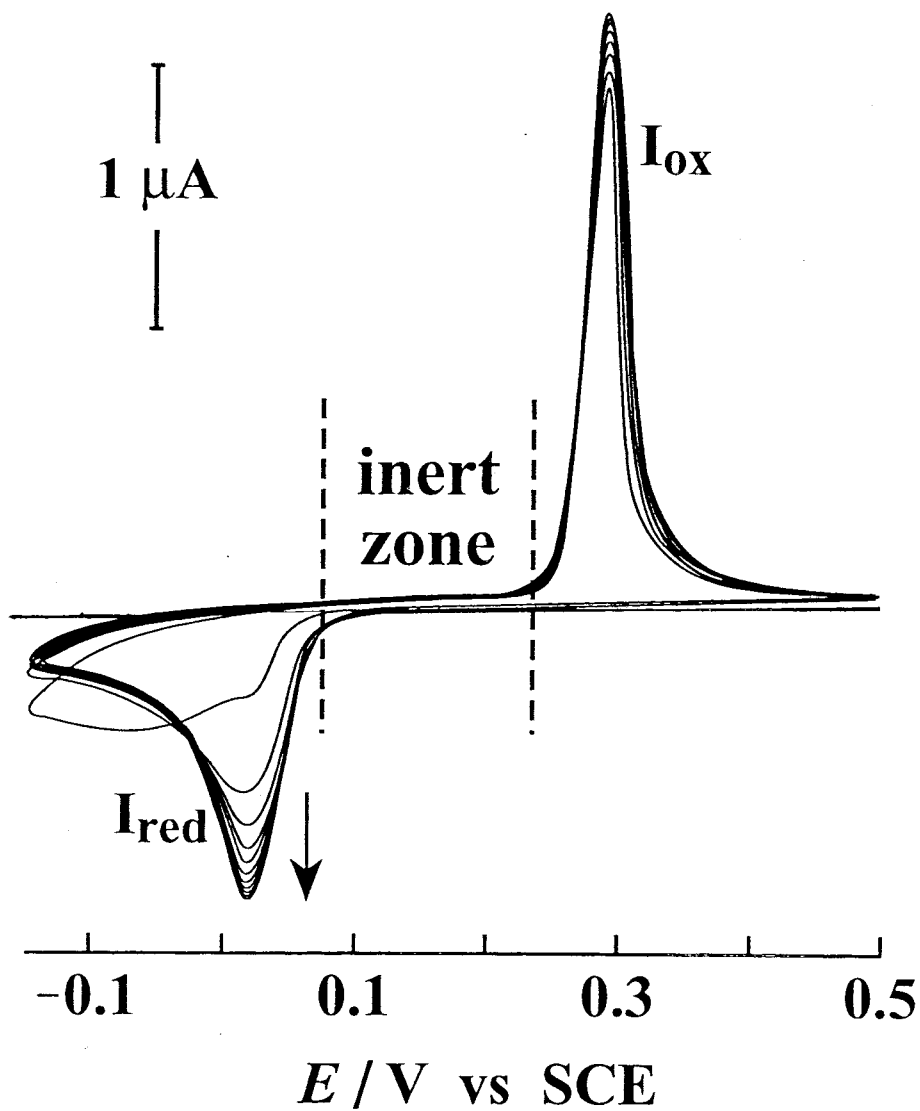


Figure 1.3. Solid state voltammetric response of nanocrystals of TCNQ trapped beneath a freshly-prepared layer of Nafion on a RAMTM electrode immersed in 1M KCl(aq) [scan rate of 100 mV s⁻¹, solution flow rate of 1 ml min⁻¹] [3-4]

In the [TCNQ]^{0/-} reaction, the solid state voltammetry is governed by nucleation and growth kinetics. Figure 1.4, shows the work associated with the formation of a spherical crystal as calculated using the formula:

$$\Delta G = G_v \frac{4\pi r^3}{3} + \gamma 4\pi r^2 \quad (1.7)$$

where G_v is the Gibbs free energy per unit volume, r is the radius of the sphere, and γ is surface free energy per unit area.

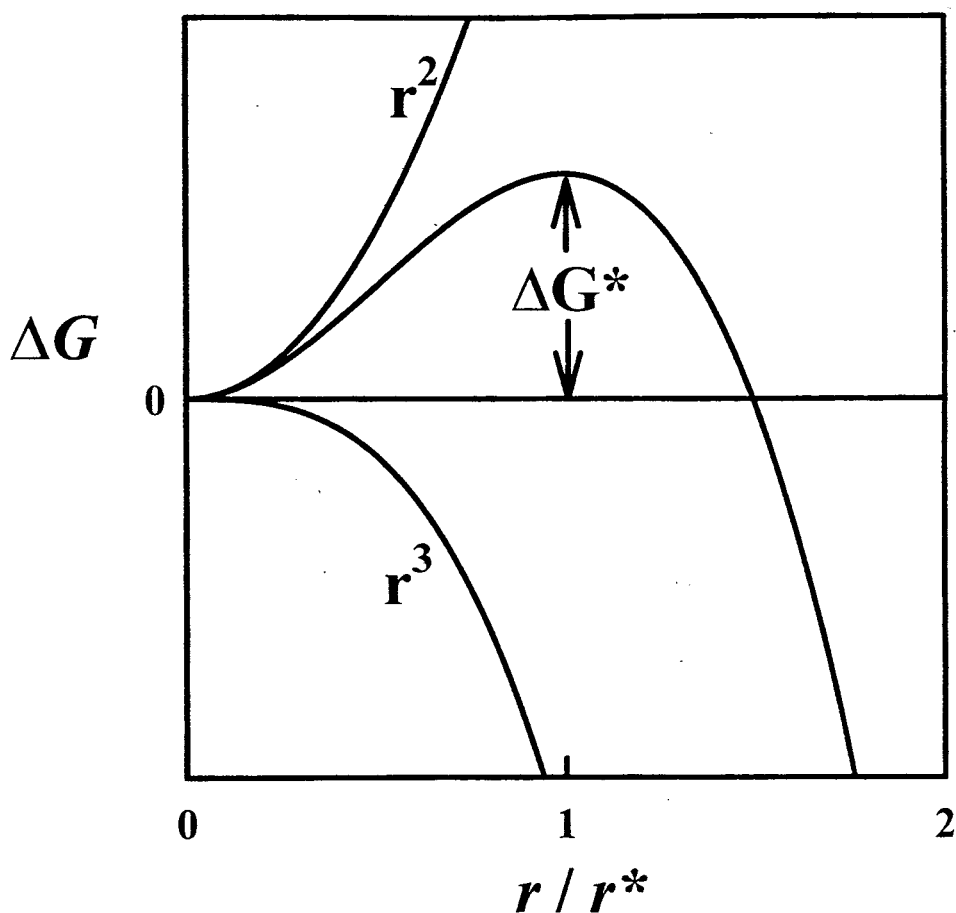


Figure 1.4. The work associated with the formation of a crystal. The resulting curve passes through a maximum at the critical radius r^* . [8]

The first term in equation 1.7 is an energy term for the work of formation of the volume of the crystal. This energy is negative and consequently favours formation. However, the second term in the equation is positive and relates to the energy cost of forming a new surface. The first term is proportional to r^3 (volume), whereas the second term is proportional to r^2 (area). Initially the r^2 term dominates which means a crystal of critical radius has to be formed before growth of the crystal is favourable. This is the origin of the large inert zone seen in Figure 1.3. An overpotential must be applied in order to supply the system with enough energy (ΔG^*) to nucleate a crystal.

A diagnostic tool can be used to determine whether nucleation and growth kinetics prevail. This involves prematurely switching the potential at the foot of the reduction or oxidation wave (see Figure 1.5). It is seen in both cases even though the driving force (the potential) is being reduced the current continues to increase forming what is known as a nucleation or inductive loop [10]. The current continues to increase because the surface area of the crystal is increasing at a faster rate than the driving force is being reduced. Consequently observation of this loop provides a test for control by nucleation and growth kinetics.

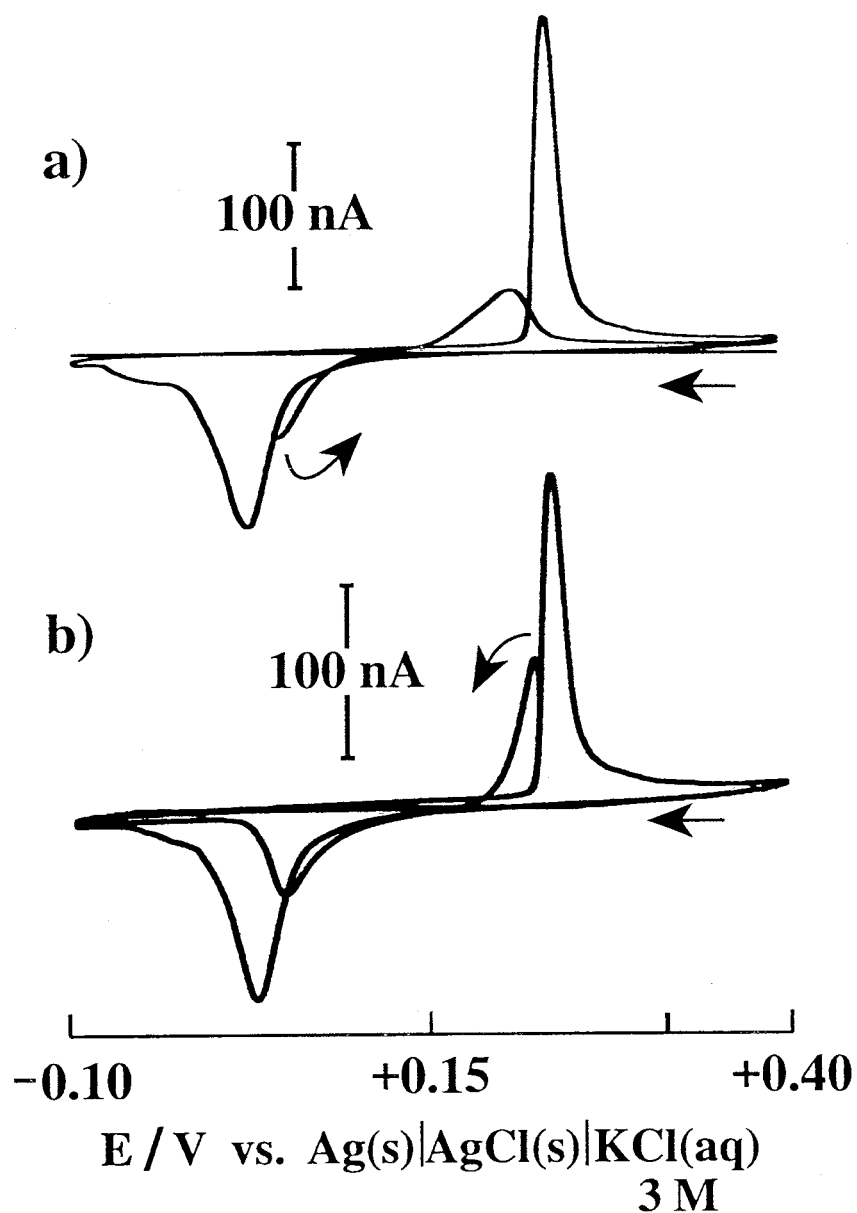


Figure 1.5. Cyclic Voltammograms for nanocrystals of TCNQ immobilized on a Nafion-coated RAM electrode in 0.01M NaCl(aq) [scan rate of 100 mV s^{-1}]. Two cycles are shown in which the scan directions are reversed at potentials corresponding to the foot of a) the reduction and b) the re-oxidation. [4]

1.4.2. Non-nucleating systems. The TCNQ system described above typically involves 100% conversion of compound (as long as the counter ion is small enough to penetrate the structure). However, many systems are not governed by nucleation and growth kinetics and only are fractionally oxidised or reduced. It is assumed for these systems that the reaction begins at the surface exposed to both solution and electrode and spreads over the surface. The reaction then proceeds to a limited depth of the crystal. Such a system is illustrated in Figure 1.6. The peak to peak separation of these systems can vary widely from around 0 mV to 300 mV.

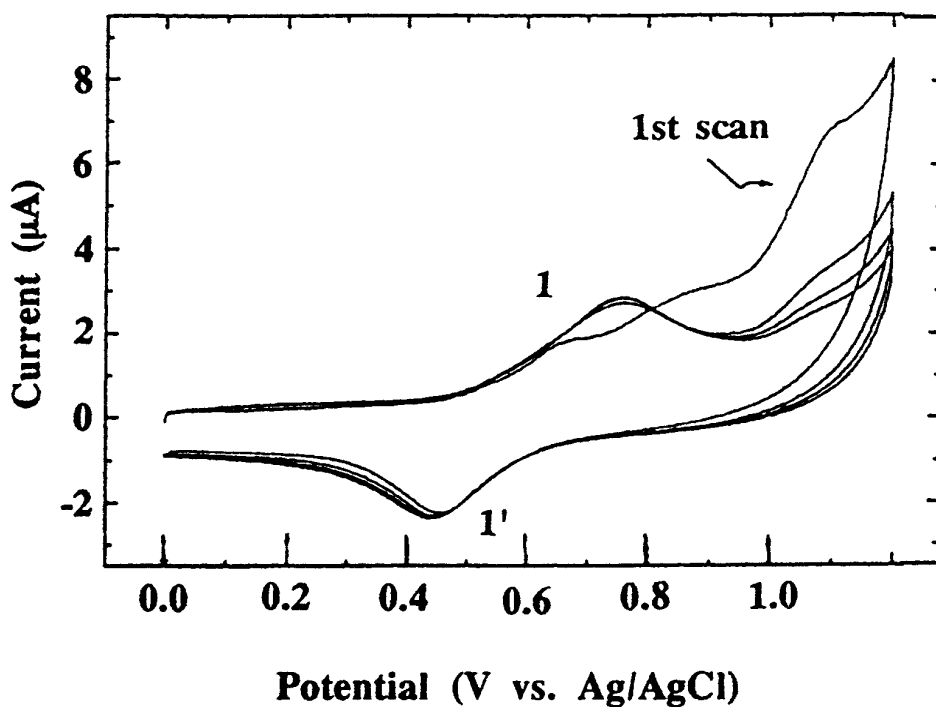


Figure 1.6. Cyclic Voltammogram (scan rate of 10 mV/s) for solid *trans*- $\text{Re}(\text{CO})(\text{dppe})_2\text{Br}$ attached to a graphite electrode immersed in water (0.1M NaClO_4). Scan rate of 100 mV s^{-1} . [11]

1.5. Double Step Chronoamperometry or Chronocoulometry. This technique involves firstly setting the potential to a rest potential, E_{rest} , where no Faradaic reaction takes place and consequently no significant current flows. The potential is then switched to a potential E_{forward} , which is forward of the redox potential of the compound of interest. The potential is held for a fixed time and then typically switched back to the rest potential and held for a preset time (see Figure 1.7).

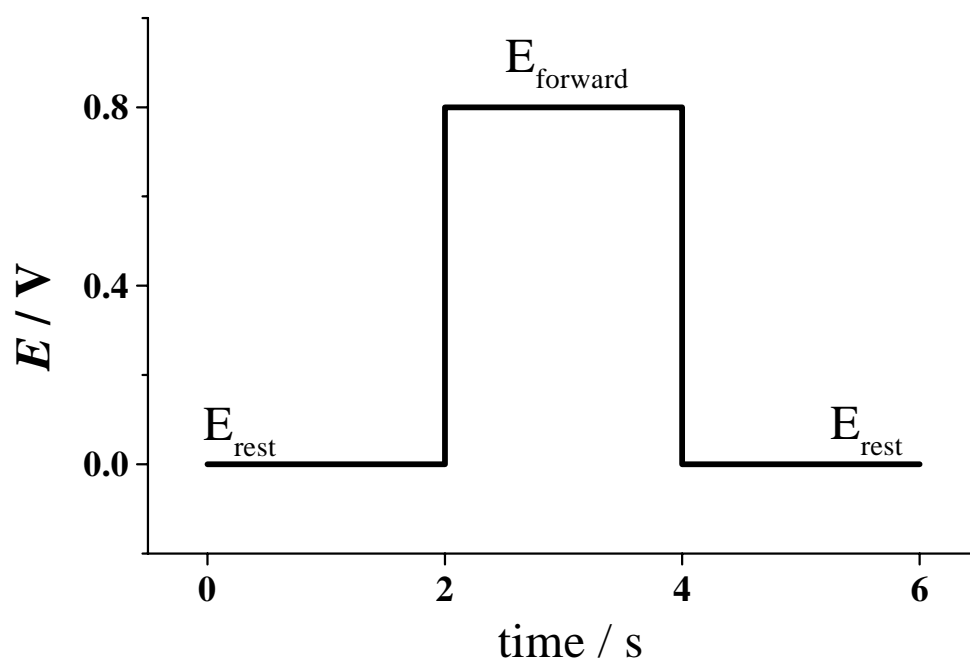


Figure 1.7. Potential Waveform for Double Step Chronoamperometry or Chronocoulometry.

When solution phase reactions are considered, the decay of faradaic current, when the potential is stepped to E_{forward} is described by the Cottrell equation [12]:

$$I_f(t) = \frac{nFAD^{1/2}c_0}{\pi^{1/2}t^{1/2}} \quad (1.8)$$

Where n is the number of electrons, F is the Faraday's constant (C mol^{-1}), A is the area of the electrode (cm^2), D is the diffusion coefficient (cm^2s^{-1}) c_0 is the bulk concentration of the analyte (mol cm^{-3}), and t is the time (s)

This technique is called chronoamperometry and in integrate form chronocoulometry. When the potential is stepped back to the initial value the terms double step chronoamperometry and chronocoulometry apply.

There is also a capacitive component of the current which decays exponentially in time according to the following equation [12]:

$$I_c(t) = \frac{\Delta E}{R} e^{-\frac{t}{RC}} \quad (1.9)$$

Here R = resistance (ohms), C = capacitance (F).

This capacitive current decays rapidly and therefore is only significant when looking at short times.

A chronocoulometric plot used in this thesis, the Anson plot [12], is useful to determine if the process is diffusion controlled. The plot is of charge versus the square root of time and should result in a straight line for a diffusion controlled process. The equation governing this process, assuming no capacitive charge and no adsorbed species is [12]:

$$Q = 2nFAc_0 \left(\frac{Dt}{\pi} \right)^{1/2} \quad (1.10)$$

The effect of adsorption can easily be detected using the Anson plot, as significant deviations from equation 10 occur. If crystal growth reactions occur, then again a characteristic response will be detected. These cases will be explained in Chapter 7.

1.6. The Electrochemical Quartz Crystal Microbalance. In solid state voltammetry, mass changes occur at the electrode surface as oxidation and reduction occur. The quartz crystal microbalance utilises the piezoelectric [13-16] qualities of quartz crystals to measure changes in the attached surface mass. Figure 1.8, shows a schematic representation of the electrochemical quartz crystal microbalance (EQCM) instrumentation. In the electrochemical application, the quartz crystal is coated with a gold disc on both sides. One side is exposed to the solution in the electrochemical cell, while the other is exposed to air. Voltammetry is carried out using the gold disc exposed to solution as the working electrode. This EQCM setup allows simultaneous measurement of mass and current in a voltammetric

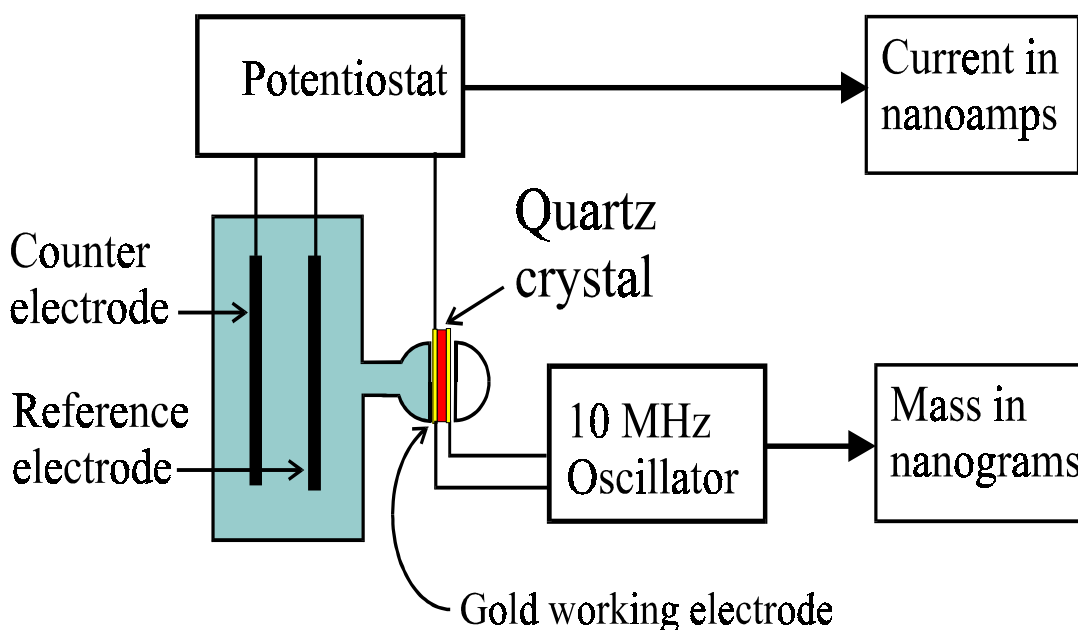


Figure 1.8. Schematic diagram of Quartz Crystal Microbalance instrumentation. (crystal is held between two o-rings)

experiment. The first *in situ* application of the QCM to electrochemistry was by Nomura and co-workers [17,18] for Cu[II] and Ag[I] electrodeposition.

The inverse piezoelectric effect is key to the operation of the quartz crystal microbalance. The application of an electric field to the quartz crystal causes a shear deformation (strain). Figure 1.9a, illustrates the shear deformation (parallel to the gold surface). This deformation arises from the realigning of dipoles in the crystal structure with the applied electric field. This deformation is typically 10-100 nm, for AT-cut crystals operating in the frequency range of 1-10 MHz, [19-22]. Figure 1.9b, illustrates a side 2D view of the shear deformation.

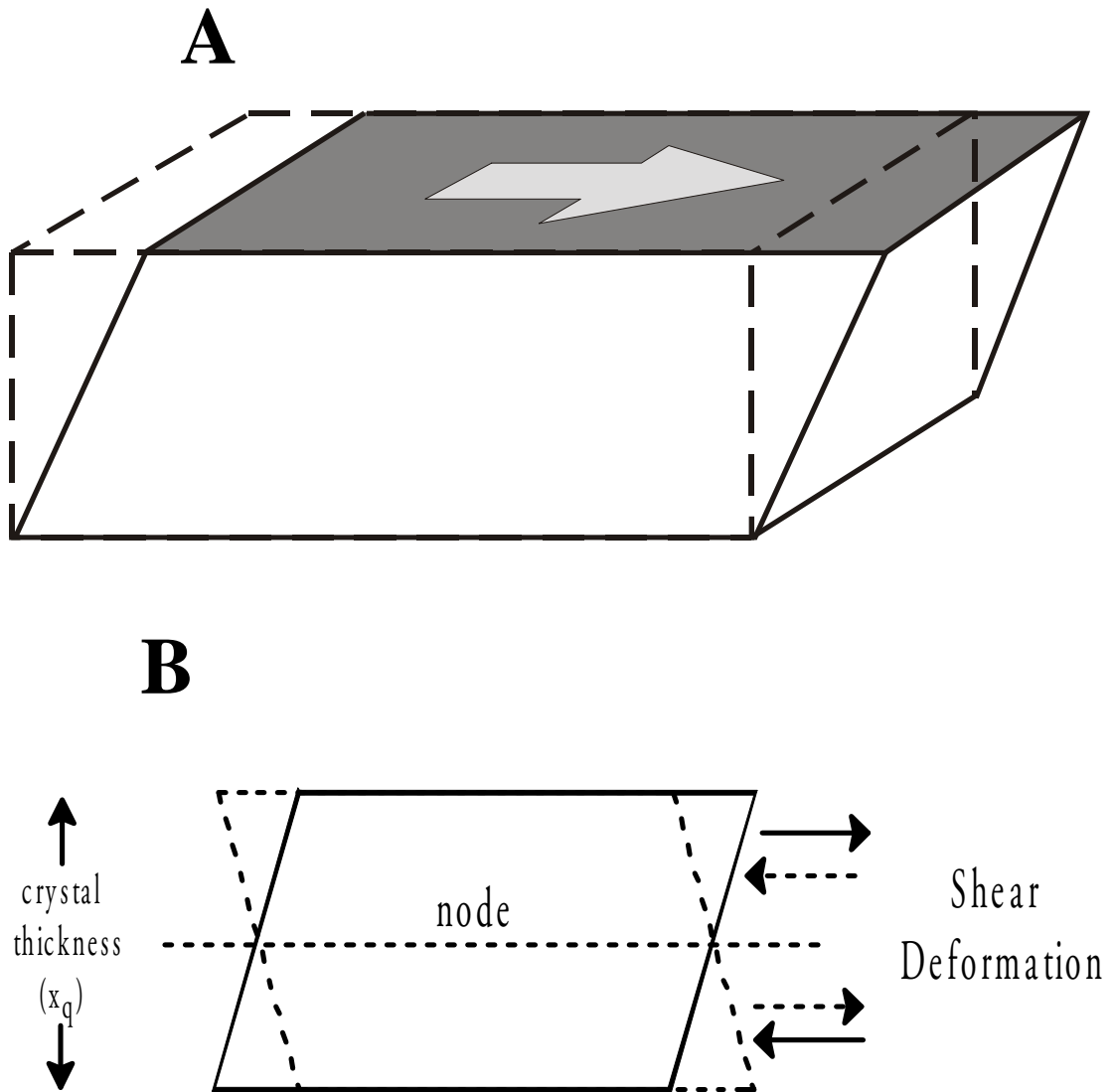


Figure 1.9. a) Illustration of shear deformation. b) Side view of crystal oscillating in an alternating electric field.

The application of an alternating electric field at a characteristic frequency $f_0(m)$ to a quartz crystal of mass m causes it to resonate:

$$f_0(m) = \frac{\sqrt{\mu_q}}{2x_q \sqrt{\rho_q}} \quad (1.11)$$

where μ_q is the shear modulus of the quartz crystal (2.947×10^{11} dyne cm^{-2} for AT-cut quartz), ρ_q is the density of quartz (2.648 g cm^{-3}) and x_q is the thickness of the quartz.

The quartz is cut to a thickness of around 0.17mm in order for it to resonate at a frequency of 10 ± 0.05 MHz. Deposition of the gold (working electrode) layer dampens the resonant frequency. When the gold quartz crystal electrode is placed in the aqueous solution the resonant frequency is viscously damped via the following equation [23]:

$$\Delta f_0 = -2.26 \times 10^{-6} f_0(0)^{3/2} (\eta_L \rho_L)^{1/2} \quad (1.12)$$

where η_L is the conventional viscosity of the liquid and ρ_L is the density of the liquid.

Also rigid attachment of mass to the gold surface will damp this frequency. The Sauerbrey equation [19] relates the damping of frequency (Δf_0) to the change in surface attached mass (Δm), assuming a thin, uniform, rigidly attached mass:

$$\begin{aligned} \Delta f_0 &= f_0(m + \Delta m) - f_0(m) \\ &= -\left(\frac{f_0(m)}{A x_q \rho_q}\right) \Delta m = -S \Delta m \end{aligned} \quad (1.13)$$

where Δm is the change in surface mass, A is the piezoelectrically active area and S is the Sauerbrey constant.

1.7. In-lens Field Emission Scanning Electron Microscopy (IFESEM). Structural information on solids attached to an electrode surface are required in solid state voltammetric studies. The IFESEM method was used for this purpose in this thesis. A scanning electron microscope uses electrons rather than light to observe the microstructure of samples. The wavelength of electrons is much less than light allowing greater resolution and magnification.

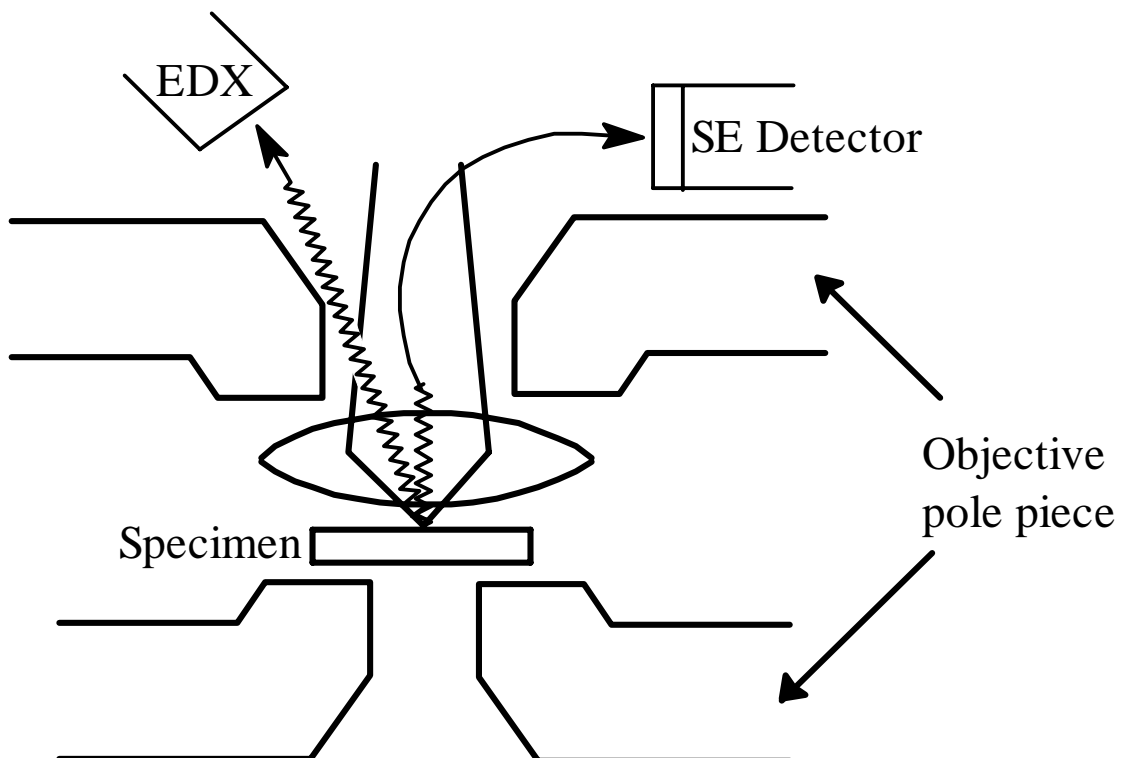


Figure 1.10. Schematic Diagram of IFESEM setup [24].

In an In-lense Field Emission Scanning Electron Microscope the specimen is placed inside the objective lens gap as shown in Figure 1.10 [24]. Conventional SEM devices have the specimen outside of the objective lens. This setup provides for significant improvement in spherical and chromatic aberrations, allows for the finely focussing of the beam onto the specimen and produces 0.6 nm resolution.

1.8. X-ray Diffraction. Another structural tool used in this thesis is X-ray diffraction. The technique was applied to both single crystals and powders. X-rays are high energy / short wavelength forms of electromagnetic radiation. The wavelengths are of the order of atomic spacings allowing them to be used to probe crystal structures. X-ray diffraction [13-14] is illustrated in Figure 1.11. If the extra distance the wave has to travel to strike the next row of atoms (A->B->C) in Figure 1.11) is an integer value of the wavelength of the x-rays then constructive interference will occur. Thus the condition for diffraction is:

$$n\lambda = \overline{AB} + \overline{BC} \tag{1.14}$$

$$n\lambda = 2d \sin(\theta) \tag{1.15}$$

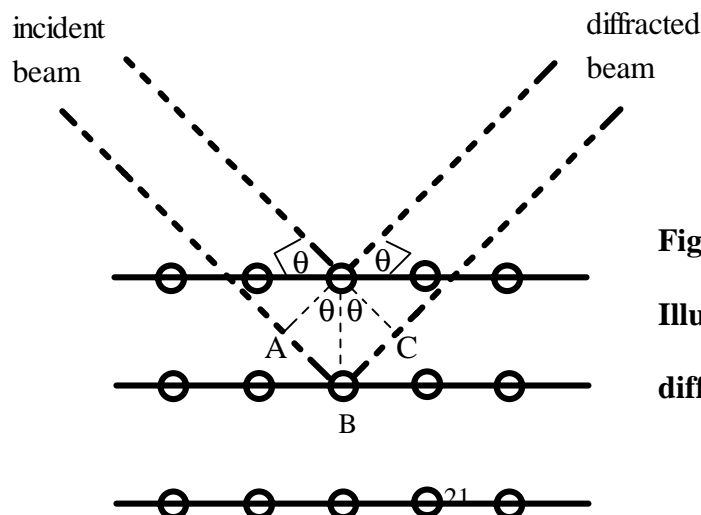


Figure 1.11.
Illustration of X-ray
diffraction.

Equation 14 is known as Bragg's Law. If Bragg's law is not obeyed then non-constructive interference will occur resulting in a very low intensity diffracted beam. Therefore d is measured from the peaks of intensity. Structures of a single crystal may be determined from X-ray diffraction data on the single crystal.

Powder Diffraction involves the use of a powdered specimen, which consists of many fine and randomly oriented particles. Some of which will be correctly oriented to satisfy the Bragg correlation (1.15) The instrumentation is illustrated in Figure 1.12. The X-ray source fires x-rays at the specimen. The moveable detector then counts X-rays at an angle 2θ . A diffraction pattern is produced for a range of 2θ values and again structural information emerges from the interpretation of the data.

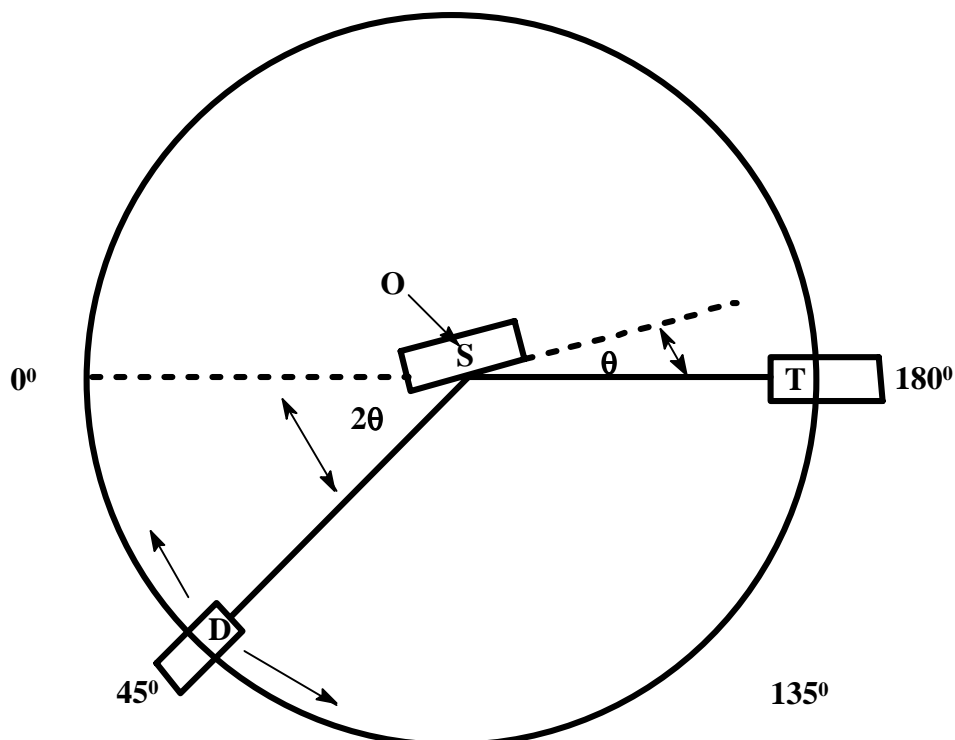


Figure 1.12. Schematic diagram of an x-ray diffractometer. T = x-ray source, S = specimen, D = detector and O = axis about which specimen and detector rotate.

1.9. Molecular Modelling.

Using atomic co-ordinates obtained from single crystal XRD measurements molecular modelling can be carried out using a computer program. This program allows a three dimensional visualisation of the crystal structure to be observed. This structure can be rotated and manipulated at will. Also the crystal can be built up by stacking unit cells side by side.

This molecular modelling can be very useful in studying changes upon oxidation or reduction. These can give an idea of the mechanism or pathway by which ions intercalate. Ion channels can be observed using molecular modelling. Also, as is the case in Chapter 6, the mechanism by which solvent inclusion occurs can be studied using molecular modelling. Here hydrophobic channels were observed in the starting compound, which are theorised to be the channels through which the solvent enters the structure.

1.10. References.

- [1] Kissinger, P.T.; Heineman, W.R., *J. Chem. Edu.*, **1983**, 60(9), 702-706
- [2] Rudolph, M.; Reddy, D.; Feldberg, S. W. *Anal. Chem.* **1994**, 66, 589A.
- [3] Bond, A.M.; Fletcher, S.; Symons, P.G., *Analyst*, **1998**, 123, 1891-1904.
- [4] Bond, A.M.; Fletcher, S.; Marken, F.; Shaw, S.J.; Symons, P.G., *J. Chem. Soc. Faraday Trans.*, **1996**, 92(20), 3925-3933
- [5] Evans, C.D.; Chambers, J.Q., *Chem. Mater.*, **1994**, 6, 454-460
- [6] Evans, C.D.; Chambers, J.Q., *J. Am. Chem. Soc.* **1994**, 116, 11052-11058
- [7] Suarez, M.F.; Bond, A.M.; Compton, R.G., *J. Solid State Electrochem.*, **1999**, 4, 24-33.
- [8] Fletcher, F.; Horne, M.D., *Electrochem. Comm.*, **1999**, 1, 502-512
- [9] Symons, P.G., *PhD Thesis*, **1998**
- [10] S. Fletcher, C.S.Halliday, D. Gates, M. Westcott, T. Lwin and G.Nelson, *J Electroanal. Chem.*, **1983**, 159, 267-285
- [11] Bond, A.M.; Colton, R.; Humphrey, D.G.; Mahon, P.J.; Snook, G.A.; Tedesco, V.; Walter, J.N., *Organometallics*, **1998**, 17(14), 2977-2985
- [12] Bard, A.J.; Faulkner, L.R., *Electrochemical Method, Fundamentals and Applications*, Wiley: New York, **1980**; p 935 and references therein.
- [13] Callister, W.D., “*Materials Science and Engineering: An Introduction. Second Edition*” , **1985**, John Wiley and Sons, Brisbane
- [14] Ruoff, Arthur L., “*Materials Science*” , **1973**, Prentice-Hall, New Jersey
- [15] Bottcher, C.J.F., “*Theory of Electric Polarisation*” , **1952**, Elsevier Publishing Company, London

- [16] **Bunget, I.; Popescu, M.**, “*Physics of Solid Dielectrics*”, **1984**, Elsevier Publishing Company, Oxford
- [17] **Nomura, T.; Nagamune, T.; Izutsu, K.; West, T.S.**, *Bunseki Kagaku*, **1981**, 30, 494
- [18] **Nomura, T.; Iijima, M.**, *Anal Chim Acta*, **1981**, 131, 97
- [19] **Sauerbrey, G.**, *Z. Physik*, **1959**, 155, 206-222
- [20] **Bahadur, H.; Parshad, R.**, in *Physical Acoustics, Vol 16* (W.P. Mason and R.N. Thurston, eds.), Academic Press, New York, **1982**, 37-171.
- [21] **Sauerbrey, G.**, *Proc. Annu. Freq. Control Symp.*, **1967**, 21, 63
- [22] **Buttry, D.A.**, “Applications of the Quartz Crystal Microbalance to Electrochemistry”, from *Electroanalytical Chemistry: A Series of Advances Vol 17*, edited by Alan J. Bard
- [23] **Brukenstein, S.; Shay, M.**, *Electrochimica Acta*, **1985**, 30(10), 1295-1300
- [24] The Hitachi S-5000 field emission SEM brochure